Bcl-x_L increases mitochondrial fission, fusion, and biomass in neurons

Sarah B. Berman,[1,3,5] Ying-bei Chen,[4] Bing Qi,[1] J. Michael McCaffery,[6] Edmund B. Rucker III,[7] Sandra Goebbels,[8] Klaus-Armin Nave,[8] Beth A. Arnold,[5] Elizabeth A. Jonas,[9] Fernando J. Pineda,[1,2] and J. Marie Hardwick[1,3,4]

[1]W. Harry Feinstone Department of Molecular Microbiology and Immunology, and [2]Department of Biostatistics, Bloomberg School of Public Health, Johns Hopkins University, Baltimore, MD 21205
[3]Department of Neurology and [4]Department of Pharmacology and Molecular Sciences, Johns Hopkins School of Medicine, Baltimore, MD 21205
[5]Department of Neurology, Pittsburgh Institute for Neurodegenerative Diseases, University of Pittsburgh, Pittsburgh, PA 15260
[6]Department of Biology, and the Integrated Imaging Center, Johns Hopkins University, Baltimore, MD 21218
[7]Animal Sciences Unit, University of Missouri, Columbia, MO 65211
[8]Department of Neurogenetics, Max-Planck-Institute of Experimental Medicine, D-37075 Goettingen, Germany
[9]Department of Internal Medicine, Yale University, New Haven, CT 06520

Mitochondrial fission and fusion are linked to synaptic activity in healthy neurons and are implicated in the regulation of apoptotic cell death in many cell types. We developed fluorescence microscopy and computational strategies to directly measure mitochondrial fission and fusion frequencies and their effects on mitochondrial morphology in cultured neurons. We found that the rate of fission exceeds the rate of fusion in healthy neuronal processes, and, therefore, the fission/fusion ratio alone is insufficient to explain mitochondrial morphology at steady state. This imbalance between fission and fusion is compensated by growth of mitochondrial organelles. Bcl-x_L increases the rates of both fusion and fission, but more important for explaining the longer organelle morphology induced by Bcl-x_L is its ability to increase mitochondrial biomass. Deficits in these Bcl-x_L–dependent mechanisms may be critical in neuronal dysfunction during the earliest phases of neurodegeneration, long before commitment to cell death.

Introduction

Mitochondrial dysfunction is implicated in many neurodegenerative diseases and other human maladies (Wallace, 1999; Chan, 2006; Dimauro and Schon, 2008). Mitochondria are actively transported through axons and dendrites, and can localize at synapses, where they may contribute critical functions required for proper neuronal activity such as ATP production, calcium handling, and the biosynthesis of α-ketoglutarate, the neurotransmitter glutamate, and other metabolites (Nicholls and Ferguson, 2002; Verstreken et al., 2005; Boldogh and Pon, 2007). Mitochondria can also contribute to programmed cell death, and Bcl-2 family members are well-known regulators of the mitochondrial step during apoptotic death, a late-stage event that can occur long after deterioration of critical neuronal functions (Bredesen, 2008). Attention has been focused primarily on the mechanisms by which anti- and pro-death Bcl-2 family proteins interact with each other to regulate outer mitochondrial membrane permeability during apoptosis, superseding the study of Bcl-2 proteins in healthy cells (Adams and Cory, 2007; Basanez and Hardwick, 2008; Chipuk and Green, 2008). However, there is growing evidence that Bcl-2 proteins influence mitochondrial morphology and localization in healthy cells, and can modulate synaptic activity in healthy neurons, potentially influencing the initial steps in neurodegeneration (Fannjiang et al., 2003; Jonas et al., 2003; Karbowski et al., 2006). The mechanisms by which Bcl-2 family proteins alter neuronal function could be linked to their effects on mitochondrial fission and fusion, dynamic processes that are increasingly linked to neuronal function and neurodegeneration (Frank, 2006; Detmer and Chan, 2007; Knott et al., 2008).

A balance between fission and fusion is generally thought to determine mitochondrial morphology in both healthy and dying cells, which is consistent with elegant genetic studies in

Correspondence to J. Marie Hardwick: hardwick@jhu.edu

Abbreviations used in this paper: cKO, conditional knockout; DIV, days in vitro; dn, dominant negative; DrOF, direct observation of fission/fusion; E, embryonic day; mtPA-GFP, mitochondria-targeted photoactivatable-GFP; mtRFP, mitochondria-targeted red fluorescent protein; VDAC, voltage-dependent anion channel.

The Rockefeller University Press $30.00
J. Cell Biol. Vol. 184 No. 5 707–719
www.jcb.org/cgi/doi/10.1083/jcb.200809060

yeast (Shaw and Nunnari, 2002). The proteins that carry out mitochondrial fission and fusion are best characterized in yeast, but the mammalian homologues identified thus far appear to operate by similar mechanisms (Okamoto and Shaw, 2005; Hoppins et al., 2007). The fission factor Drp1/DLP1/Dnm1 is a large GTPase that is recruited to mitochondria via membrane-anchored proteins that may include Fis1 and Mff to form complexes that decorate the mitochondrial surface (James et al., 2003; Yoon et al., 2003; Schauss et al., 2006; Gandre-Babbe and van der Bliek, 2008). Regulated in part by posttranslational modifications, it appears that fission occurs when GTP-bound Drp1 oligomerizes, constricts organelles, and dissociates upon GTP hydrolysis (Bhar et al., 2006; Hoppins et al., 2007; Knott et al., 2008). Distinct dynamin-like GTPases, including Mfn2 (mitofusin 2) on the outer membrane and Opa1 (optic atrophy-1) on the inner membrane, mediate fusion of two mitochondria into a single organelle (Cerveny et al., 2007; Detmer and Chan, 2007). Genetic mutations in these mitochondrial fusion factors cause human neuropathies and have been linked recently to brain lesions and stroke, and a mutation in Drp1 was described in an infant with fatal abnormal brain development (Zuchner et al., 2004; Frank, 2006; Waterham et al., 2007; Chung et al., 2008).

The antiapoptotic mammalian Bcl-2 family protein Bcl-x_L, and its *Caenorhabditis elegans* counterpart CED-9, localize to mitochondria and are required for normal development of the nervous system and other compartments (Motoyama et al., 1995; Shaham and Horvitz, 1996). Bcl-x_L and CED-9 were previously implicated in facilitating mitochondrial fusion through an interaction with Mfn2 (Delivani et al., 2006). However, a role for Bcl-x_L and CED-9 in mitochondrial fission is also supported by the interaction of Bcl-x_L with Drp1 (Li et al., 2008) and by genetic studies in worms (Jagasia et al., 2005). Although Bcl-x_L is abundantly expressed in healthy adult neurons (Krajewski et al., 1994), the effects of Bcl-x_L on mitochondrial dynamics in neurons are largely unexplored.

In addition to its role in healthy neurons, Drp1 also makes an important contribution to the mitochondrial fission/fragmentation that is characteristic of apoptotic mammalian cells (Frank et al., 2001; Breckenridge et al., 2003). Drp1 and its homologues in flies, worms, and yeast can also enhance cell death, which implies a conserved pro-death function of Drp1/Dnm1 (Fannjiang et al., 2004; Jagasia et al., 2005; Goyal et al., 2007). This function of Drp1 may involve Bcl-2 family proteins such as proapoptotic Bax and Bak, which also promote fragmented mitochondrial morphologies during apoptosis and colocalize with both Drp1 and Mfn2 on mitochondria (Karbowski et al., 2002). In sharp contrast to dying cells, Bax and Bak promote mitochondrial fusion in healthy cells and protect against neuronal cell death under some conditions (Lewis et al., 1999; Fannjiang et al., 2003; Karbowski et al., 2006). In yet another twist, CED-9, the essential anti-death Bcl-2 protein in worms, can also promote Drp1-dependent cell death in worms (Jagasia et al., 2005), and Bcl-x_L can be detrimental to synaptic transmission based on the ability of ABT-737, a small molecule inhibitor of Bcl-x_L, to inhibit hypoxia-induced synaptic rundown in the squid stellate ganglion (Hickman et al., 2008). These seemingly conflicting results could imply that fission/fusion factors and Bcl-2 family proteins coregulate a delicately balanced process.

Drp1-mediated fission may facilitate cell survival by producing new mitochondria and removing damaged sections of mitochondria that are promptly degraded, whereas excessive fission mediated by Drp1 after a death stimulus may promote mitochondrial dysfunction, damage, or accelerated degradation. However, several lines of evidence suggest that the fission function of Drp1 is biochemically distinct from its cell death function (Parone et al., 2006; Cassidy-Stone et al., 2008). Less clear are the detailed mechanisms involved in Bcl-x_L–induced, Drp1-dependent mitochondrial localization to presynaptic boutons that facilitate synaptic activity in dendrites and axons (Li et al., 2004; Li et al., 2008).

To date, rates of mitochondrial fission and fusion have been inferred indirectly from diffusion rates of fluorescence within the mitochondrial network (Karbowski et al., 2004; Twig et al., 2006, 2008). However, these methods could not be applied to mitochondria in long neuronal processes because changes in mitochondrial fluorescence intensity are primarily a function of organelle transport out of the field of interest rather than organelle shape changes. Therefore, we developed methods to directly monitor and quantify fission and fusion events in live neurons expressing mitochondria-targeted photoactivatable GFP (mtPA-GFP). We found that Bcl-x_L increases the rates of both fission and fusion, but its ability to increase mitochondrial length/mass is key to explaining mitochondrial morphology. Thus, fission and fusion are integrated with the control of mitochondrial mass (biogenesis and degradation) to determine mitochondrial morphology.

Results

Bcl-x_L increases mitochondrial length in cortical neurons

Bcl-x_L is a critical survival factor, as *bcl-x* knockout mice die by embryonic day ~12.5 (E12.5), with excess neuronal and hematopoietic cell death (Motoyama et al., 1995). Therefore, to examine the role of endogenous Bcl-x_L on mitochondrial morphology in neurons, we generated conditional knockouts (cKOs) in which exons 1 and 2, which encode the N-terminal 81% of the Bcl-x_L protein, were conditionally deleted in early postmitotic neurons of the hippocampus and the brain cortex (except for interneurons) beginning at ~E12.5. This was achieved by mating floxed *bcl-x* mice (Wagner et al., 2000) with knockin mice expressing Cre recombinase driven by the neuron-specific NEX promoter (Goebbels et al., 2006). Cortical neuron cultures were prepared from mouse embryos generated from heterozygous crosses, as *bcl-x* cKO mice are infertile. Cells from individual embryos were plated separately at two different densities to compensate for explantation-induced neuronal loss of cKO neurons (see Materials and methods). Embryos were genotyped by PCR, and paired cultures of similar density were used for experiments. Depletion of Bcl-x_L protein (the only protein product of the *bcl-x* gene detected) in embryonic cortical cultures was confirmed on immunoblots and by immunofluorescence microscopy (Fig. 1, A and B). To verify the survival of *bcl-x*

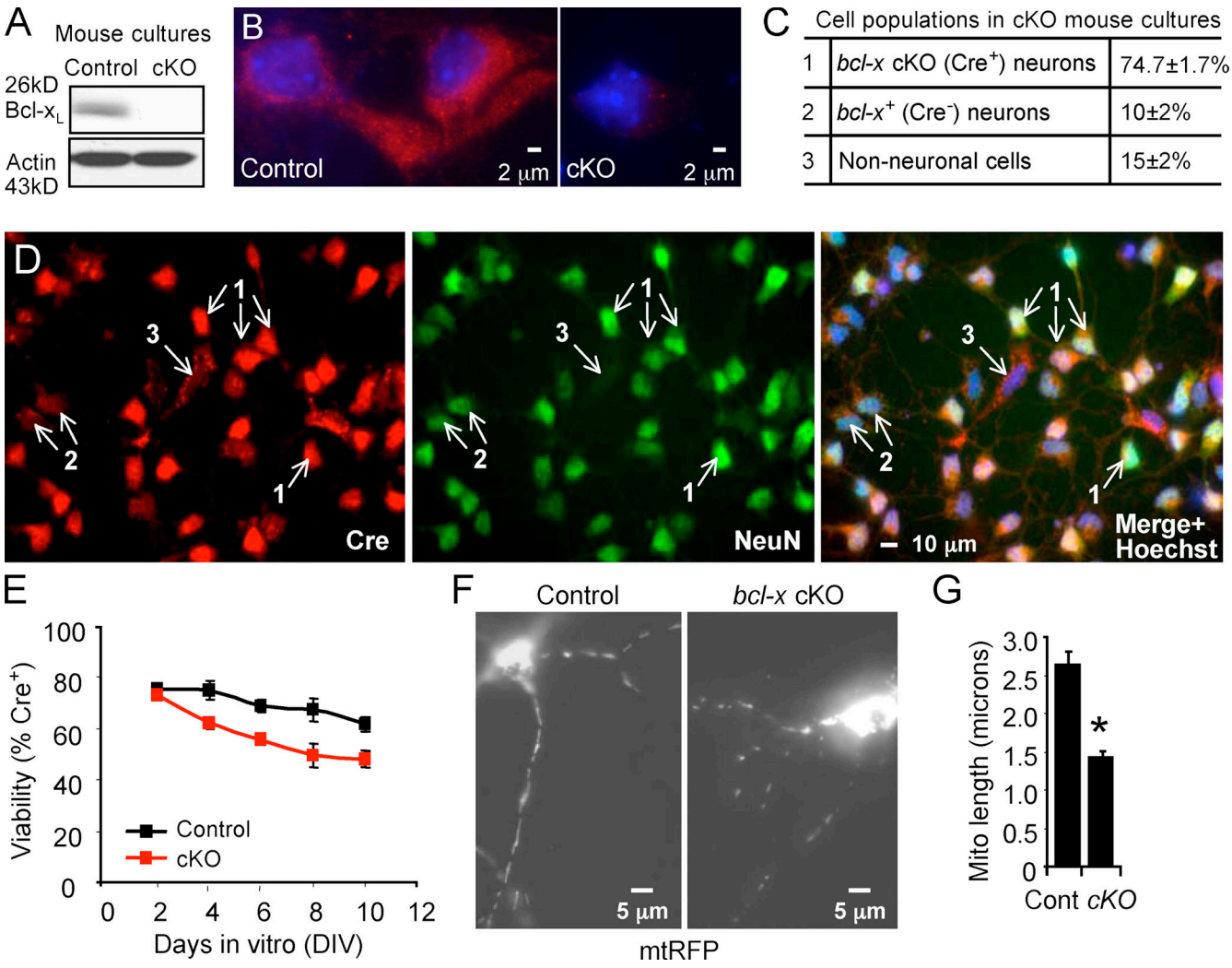

Figure 1. **Short mitochondrial morphology in mouse cortical neurons lacking Bcl-x$_L$.** (A) Representative immunoblot of control and *bcl-x* cKO cortical cultures 4 DIV confirms Bcl-x$_L$ deficiency (Boise polyclonal). (B) Immunofluorescence microscopy images show paired cortical cultures (4 DIV) stained with anti–Bcl-x$_L$ (Biocarta polyclonal, red) and with DAPI to mark cell nuclei (blue); neurons were identified by costaining with anti-NeuN (not depicted). (C) Proportions of the indicated cell types present in *bcl-x* cKO cortical neuron cultures (2 DIV) were identified by immunofluorescence microscopy as described in D and quantified; $n = 6$ samples per genotype in two independent experiments. (D) Immunofluorescence microscopy for Cre recombinase (red) and NeuN (green) in *bcl-x* cKO cortical cultures (2 DIV); Hoechst 33258 (blue) marks nuclei. Numbered arrows are defined in C. Note, both control and cKO mice have one copy of NEX replaced by Cre recombinase; only control mice contain an unfloxed copy of *bcl-x*. (E) Viability of Cre-positive neurons in *bcl-x* cKO (*bcl-x*$^{flox/flox}$;*cre*$^{+/-}$) and control (*bcl-x*$^{+/flox}$;*cre*$^{+/-}$) embryonic cortical cultures was determined by nuclear morphology with Hoechst 33258 staining in three independent experiments presented as mean ± SEM (*t* test, P = 0.01). (F) Representative images of control and *bcl-x* cKO cortical neurons (8 DIV) transfected with mito-RFP. (G) Mitochondrial length was quantified in three independent experiments as in F and presented as mean ± SEM; $n = 1{,}362$ mitochondria from 38 control neurons, and $n = 813$ mitochondria from 30 *bcl-x* cKO neurons. *t* test; *, P < 0.0001

cKO neurons, primary cortical cultures 2 d in vitro (DIV) were stained for nuclear Cre recombinase and neuron-specific NeuN (Fig. 1, C and D). Approximately 75% of the cells were *bcl-x* cKO neurons (NeuN+/Cre+; Fig. 1 D, arrow 1), and the remainder were untargeted neurons, such as interneurons (NeuN+/Cre−; Fig. 1 D, arrow 2) and nonneuronal cells (NeuN−/Cre−, Fig. 1 D, arrow 3). Although spontaneous death was elevated by 10–15% during maturation of *bcl-x* cKO neurons compared with controls, these results verify long-term survival of Bcl-x$_L$–deficient neurons in culture (Fig. 1 E).

Mitochondrial length was measured in 8-d mouse cortical cultures ~24 h after transfection with mitochondrial matrix-targeted DsRed2 (mitochondria-targeted red fluorescent protein [mtRFP]; Fig. 1 F). Neuronal processes in *bcl-x* cKO cultures had shorter and more punctate mitochondria compared with the longer tubular morphology observed in matched controls prepared from littermates, which implies that Bcl-x$_L$ leads to longer mitochondria (Fig. 1 G). Although *bcl-x* cKO neurons do not have lower mean mitochondrial membrane potentials measured with tetramethyl rhodamine methyl ester (TMRM), they exhibit greater membrane potential fluctuations (unpublished data), precluding the use of potential-sensitive dyes to accurately quantify mitochondrial morphology.

Mitochondrial morphology changes caused by increased fission are perhaps the earliest markers of declining cell health detected by light microscopy (Youle and Karbowski, 2005). Thus, despite the absence of a deliberate death stimulus and the modest differences in viability between control and *bcl-x* cKO

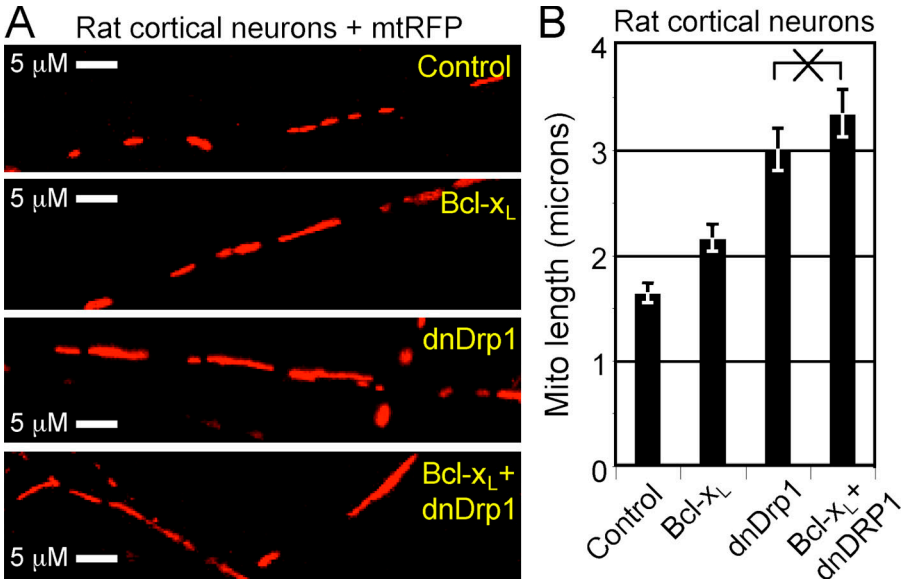

Figure 2. **Elongated mitochondrial morphology in neurons overexpressing Bcl-x_L and dnDrp1^{K38A}.** (A) Fluorescent microscopy images of rat cortical neuron processes 1 d after transfection with mito-RFP (and mtPA-GFP) plus the indicated constructs or empty vector control. (B) Data from 96–131 mitochondria in four independent experiments as shown in A were quantified and presented as mean ± SEM. All six paired comparisons are statistically different ($p < 0.001$) except dnDrp1 versus Bcl-x_L + dnDrp1 (marked with an X). See "Computational methods" and Table S1 (available at http://www.jcb.org/cgi/content/full/jcb.200809060/DC1).

cultures, we could not rule out possible indirect effects of impaired cell health on the observed punctate mitochondrial morphology in *bcl-x* cKO cells. Therefore, mitochondrial morphologies were also evaluated in 8-d rat cortical cultures ∼24 h after transfection with human Bcl-x_L (Fig. 2 A). Consistent with results from *bcl-x* knockout cultures, mitochondria were significantly elongated in neuronal processes overexpressing Bcl-x_L (Fig. 2 B), which is similar to earlier studies in mammalian cell lines and yeast (Fannjiang et al., 2004; Delivani et al., 2006). Expression of a dominant-negative mutant of mitochondrial fission factor Drp1 (dnDrp1^{K38A}) more effectively increased mitochondrial length, which was not significantly increased further by the addition of Bcl-x_L (Fig. 2, A and B). Although dnDrp1^{K38A} is assumed to act by inhibiting mitochondrial fission, morphology alone does not distinguish between inhibition of fission, induction of fusion, or other potential explanations for the effects of Bcl-x_L.

Direct measurements of mitochondrial fission and fusion using direct observation of fission/fusion (DrOF)

Mitochondrial fission and fusion capacities are often inferred from morphological shape changes, the frequency of mitochondrial encounters in living cells, and indirect methods involving fluorescence diffusion rates (Karbowski et al., 2004; Jendrach et al., 2005; Barsoum et al., 2006; Escobar-Henriques et al., 2006; Twig et al., 2006). For example, Bax and Bcl-x_L were found to increase fusion of mitochondria in healthy cells using FRAP (Delivani et al., 2006; Karbowski et al., 2006). FRAP assesses mitochondrial connectivity based on the speed with which fluorescent molecules within mitochondria refill a "bleached" area from neighboring fluorescent (unbleached) areas over several minutes to hours. More rapid recovery provides evidence of connectivity within a single mitochondrial structure. An alternative strategy for assessing mitochondrial fusion is to measure over 1–2 h the diffusion of mitochondrial photoactivated GFP away from a small subcellular region containing one or multiple fluorescent mitochondria (Karbowski et al., 2004; Twig et al., 2008). However, in long neuronal processes, changes in fluorescence intensity will more likely reflect movement of mitochondria out of the region of interest rather than fluorescence diffusion rates within a mitochondrial network, thereby compromising analysis by these methods. Therefore, to quantify mitochondrial fusion and fission events in neurons, we devised a strategy for DrOF by counting individual fission and fusion events in real time, combined with computational analyses.

To quantify fission and fusion events via DrOF, primary rat cortical neurons were cotransfected with mtRFP and with mtPA-GFP, a variant of *Aequorea victoria* GFP that fluoresces upon photoactivation at 405 nm (Patterson and Lippincott-Schwartz, 2002). Randomly distributed mitochondria detected in the red channel were selected for laser activation (Fig. 3 A). Photoactivated mitochondria instantly fluoresce green, and their fate was monitored for the next 15 min, capturing images every 10 s (Video 1, available at http://www.jcb.org/cgi/content/full/jcb.200809060/DC1). A fission event was scored when a photoactivated mitochondrion separated into two fragments with independent velocities. On rare occasions, one mitochondrion divided more than once during the 15-min observation period (Fig. 3 B and Video 2). Only 25.4% of photoactivated mitochondria had a fission event during the 15-min observation period (see Fig. 5 A, control).

A fusion event was scored only when the green fluorescence in a photoactivated mitochondrion diffused into and assumed the shape of a second (initially nonoverlapping) mitochondrion that was previously labeled only with mtRFP, verifying matrix continuity (Fig. 3 C and Videos 3 and 4, available at http://www.jcb.org/cgi/content/full/jcb.200809060/DC1). Unexpectedly, fusion events were very rare, occurring in only 8.2% of photoactivated mitochondria in 15 min (see Fig. 5 B, Control). However, this rate of fusion determined by DrOF overestimates the rate of fusion events in the mitochondrial population by exactly a factor of two (Berman et al., 2008). This is because a single fusion event is shared between two mitochondria. Accordingly, the corrected fusion rate is only 4.1% per 15 min (see Fig. 5 C).

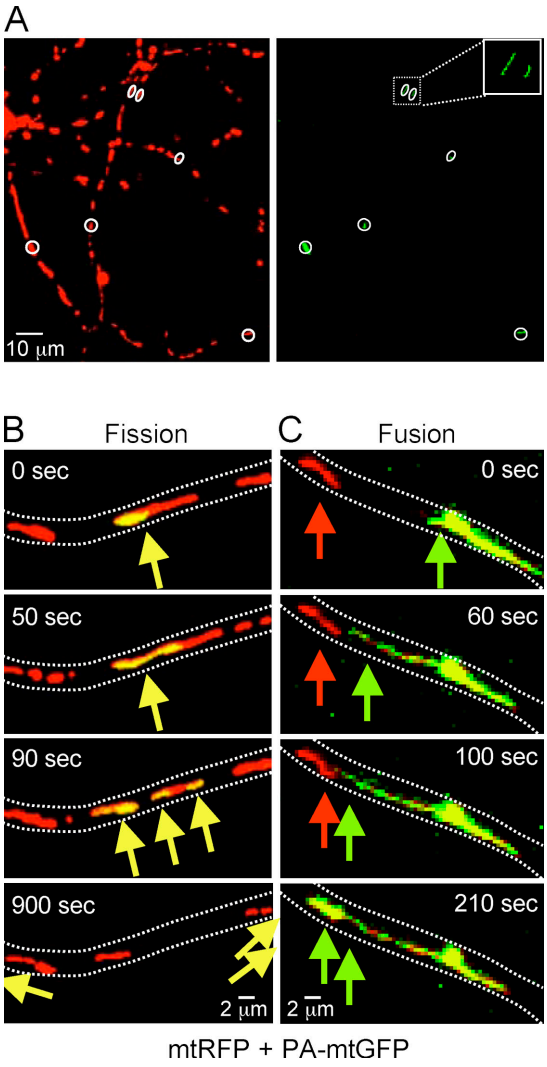

Figure 3. **High magnification time series of mitochondrial fusion and fission in neuronal processes (DrOF).** (A) Representative images of rat cortical neurons (8 DIV) cotransfected with mito-RFP and mito–PA-GFP at 7 DIV. In the red channel, mitochondria were selected for photoactivation at 405 nm (circled areas), thereby activating green fluorescence (right). (B) Selected images (merge of red and green channels) from a series of 90 frames taken at 10-s intervals reveal a rare photoactivated mitochondrion undergoing two fission events to produce three mitochondria that subsequently migrate out of view (yellow arrows). Dotted lines approximately outline the neuronal process (see Video 2, available at http://www.jcb.org/cgi/content/full/jcb.200809060/DC1). (C) Example of a photoactivated mitochondrion (green arrows) that fuses to a neighboring unactivated (red) mitochondrion (see panel B and Video 4).

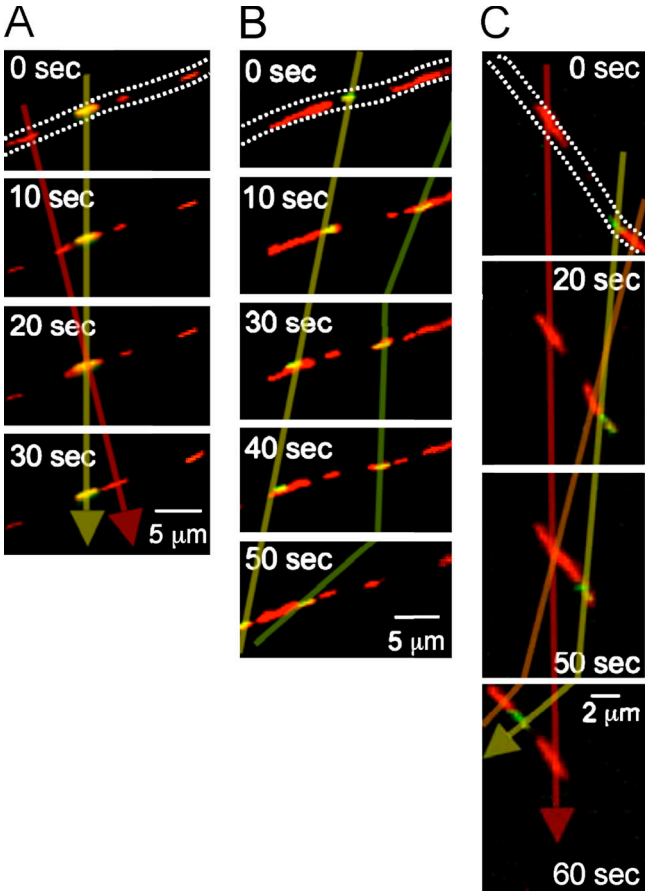

Figure 4. **Most mitochondrial encounters/visitations do not result in fusion.** (A–C) Fluorescence microscopy images of merged (red + green) channels as described for Fig. 3. Dotted lines approximately outline the neuronal processes. Transparent arrows/lines track the same mitochondrion. (A) A mitochondrion (red, not photoactivated) moves past a yellow photoactivated mitochondrion without exchanging contents. The indicated imaging times are relative to the earliest frame shown. (B) Activated (yellow) mitochondria move past stationary/slow unactivated (red) mitochondria without exchanging contents. (C) Two adjacent/overlapping mitochondria (one photoactivated) move at similar velocities without fusing to each other or to a third stationary mitochondrion.

Mitochondrial encounters rarely result in fusion

This low rate of fusion could not be attributed to low rates of mitochondrial encounters but instead was caused by the fact that only 1–2% of apparent encounters resulted in a fusion event. We commonly observed that photoactivated and unactivated mitochondria were transported past one another in the opposite (Fig. 4 A) or same direction (Fig. 4 B), or that two overlapping mitochondria were co-transported at similar rates without fusing to each other or to a stationary mitochondrion in their path (Fig. 4 C). This low rate of fusion implies that estimates based on counting apparent mitochondrial encounters are likely to dramatically overestimate mitochondrial fusion rates. The propensity to undergo a fusion event may also be dependent on the proximity of two passing mitochondria (below our limit of resolution) and on other signals based on the occasional stationary mitochondrion that appears to reach out to a nearby organelle shortly before the two undergo fusion (Video 4).

Bcl-x_L enhances both mitochondrial fusion and fission

To determine if the longer mitochondrial phenotype observed with Bcl-x_L is caused by an increased rate of fusion events, DrOF was applied to healthy cultured rat neurons. We found that Bcl-x_L overexpression significantly increased the rate of mitochondrial fusion by 2.7-fold over the vector-transfected control (Fig. 5, B and C). This finding is consistent with increased fluorescence recovery by FRAP analysis for Bcl-x_L–expressing HeLa cells (Delivani et al., 2006). Theoretically, Bcl-x_L could also increase mitochondrial length by inhibiting fission. However, no decrease in fission was observed. Instead, Bcl-x_L stimulated fission by 1.8-fold relative to control (Fig. 5 A). This Bcl-x_L–stimulated

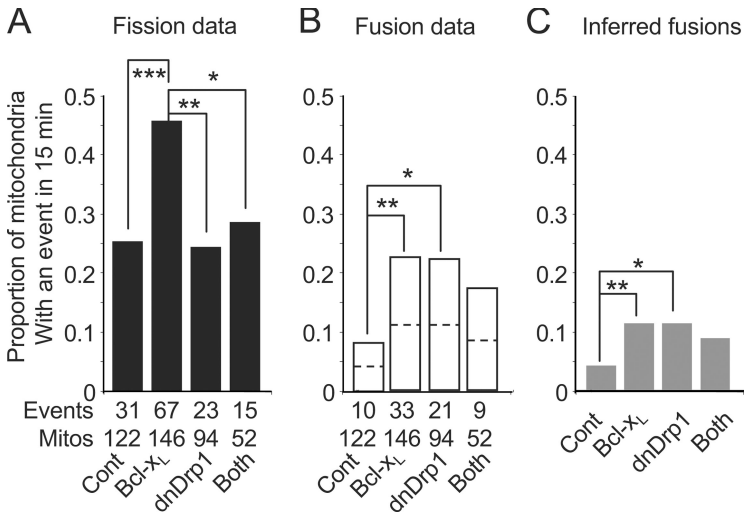

Figure 5. **Proportions of mitochondria in rat cortical neurons undergoing fission and fusion events determined by DrOF (see Fig. 3).** (A) The proportion of activated mitochondria observed to undergo fission. The total number of events for the indicated number of mitochondria was tabulated for eight independent experiments. Statistical significance was calculated using binomial tests for proportions; *, $P < 0.05$; **, $P < 0.002$; ***, $P < 0.001$. Note, the Bonferroni-corrected 95% confidence level is 0.05/6 = 0.0083. (B) The proportion of activated mitochondria observed to undergo fusion. Statistical significance was calculated using binomial tests for proportions (dashed lines are corrected by a factor of one half); *, $P < 0.007$; **, $P < 0.003$. (C) Data from B divided by factor of 2 to correct for bias caused by observation of only activated mitochondria.

fission was dependent on the mitochondrial fission factor Drp1, as cotransfection with dnDrp1^{K38A} abolished Bcl-x_L–enhanced fission. However, dnDrp1^{K38A} alone failed to suppress basal fission rates, contrary to expectation, and even more unexpectedly, dnDrp1^{K38A} increased the frequency of fusion events. Therefore, we now consider alternative interpretations to explain these data.

Drp1-containing mitochondrial fission complexes form in sparsely localized spots on the surface of mitochondria in yeast and mammalian cells (Mozdy et al., 2000; James et al., 2003; Yoon et al., 2003; Schauss et al., 2006; Amiri and Hollenbeck, 2008; Gandre-Babbe and van der Bliek, 2008). If each Drp1-binding site is equally likely to become a fission site, and if the number of binding sites is proportional to mitochondrial length as suggested, then longer mitochondria, such as those observed with Bcl-x_L or dnDrp1^{K38A}, should exhibit proportionately more fissions. That is, long mitochondria should undergo more fission events simply because they are longer, even if Bcl-x_L and dnDrp1^{K38A} have no impact on the density of Drp1-binding sites or their fission efficiency (Fig. 6 A). Indeed, when fission rates were calculated per unit length of mitochondria (based on the mean length measurements from Fig. 2 B) rather than per whole organelle, we found that dnDrp1^{K38A} significantly suppressed basal fission as predicted (Fig. 6 B). Despite recalculation of fission per unit length, Bcl-x_L was confirmed to stimulate mitochondrial fission (1.7-fold). Furthermore, Bcl-x_L–induced fission was Drp1-dependent, as dnDrp1 abolishes the effects of Bcl-x_L and further suppresses basal fission. These findings further suggest that Bcl-x_L regulates the fission function of Drp1, rather than a distinct function of Drp1 (e.g., a cell death activity; Fig. 6 C), which is consistent with reports that Bcl-x_L and CED-9 bind and activate the GTPase activity of Drp1 in vitro (Li et al., 2008; Tan et al., 2008). Collectively with the observation that Bcl-x_L stimulates mitochondrial localization to neuronal synapses and increases synapse formation, and that dnDrp1^{K38A} inhibits these effects of Bcl-x_L, we support a model where Bcl-x_L stimulates Drp1-dependent mitochondrial fission to facilitate synaptic activity (Li et al., 2008). Therefore, the abundant expression of Bcl-x_L in mature brain is likely to be critical for normal synaptic function.

Fission/fusion ratio is insufficient to explain mitochondrial morphology in mammalian neurons

A commonly held assumption is that a shift in the balance between fission and fusion is responsible for changes in mitochondrial morphology. Consistent with this assumption, a fission/fusion ratio, calculated from the rates of fission (Fig. 5 A) and fusion (Fig. 5 C) per organelle, revealed that Bcl-x_L and dnDrp1^{K38A} shift the balance toward fusion (Fig. 6 D). However, if fission and fusion are the sole determinants of mitochondrial morphology, then at steady state, their rates should be equal because theoretically a fission/fusion ratio >1 would lead to an unlimited increase in the number of very small organelles. Conversely, a fission/fusion ratio <1 would ultimately lead to a single fused organelle, as occurs in yeast lacking the gene for Dnm1/Drp1 (Shaw and Nunnari, 2002). However, neither of these situations was observed in healthy neurons or in cell lines stably expressing Bcl-x_L (unpublished data). HeLa cells overexpressing Bcl-x_L were found to display cell-to-cell differences, with cells exhibiting either fused or fragmented mitochondrial morphology (Sheridan et al., 2008). However, we did not observe excessively skewed fusion, fission, or length parameters between individual neurons. Therefore, because the rate of fission was significantly greater than the rate of fusion under all conditions analyzed by DrOF (Fig. 6 D), mitochondrial morphology at steady state cannot be explained solely by adjusting a balance between fission and fusion. Development of a more realistic description of mitochondrial morphology is necessary to invoke additional mechanisms.

Mitochondrial growth/biogenesis balances fission and fusion

The rates of fission and fusion directly affect the total number of mitochondria in a cell, given that one fission event increases the total number of mitochondria by one, and one fusion event decreases the number by one (Fig. 6 E, left). Therefore, to satisfy the conservation of total mitochondrial numbers per cell under steady-state conditions, it is necessary to invoke an alternative mechanism for eliminating the extra mitochondria generated by

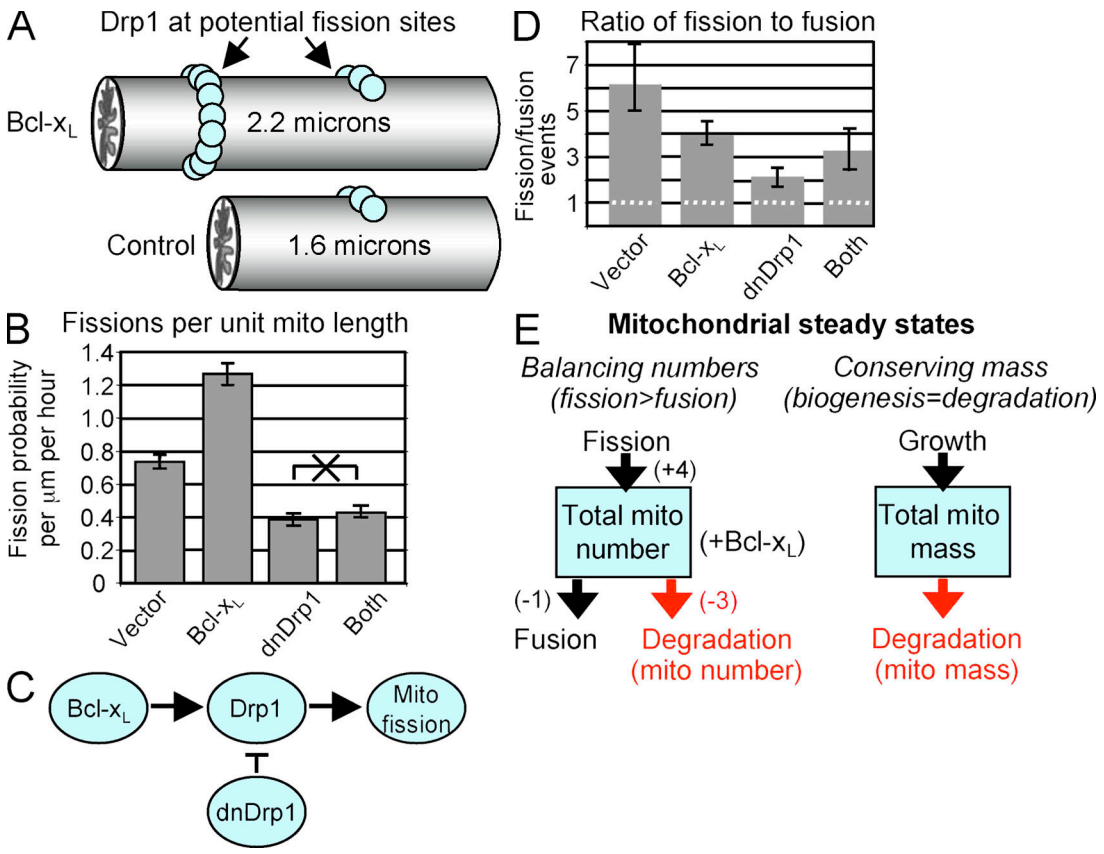

Figure 6. **Bcl-x_L induces Drp1-dependent mitochondrial fission.** (A) Diagrammatic tubular mitochondrial segments of indicated lengths corresponding to control and Bcl-x_L–expressing neurons from Fig. 2 B. These illustrate the distribution of Drp1-containing fission complexes as a function of organelle length. Drp1 molecules (balls) in complexes distributed along mitochondria mark potential sites of future fission events, which implies that the probability of a fission event is proportional to the length of the organelle, with all other conditions being constant. (B) The probability of mitochondrial fission (p_{fi}) per micrometer of mitochondrial length per hour was calculated as described in "Computational methods" (see Table S2, available at http://www.jcb.org/cgi/content/full/jcb.200809060/DC1). P = 0.0002 for all six paired comparisons except for dnDrp1 versus dnDrp1+ Bcl-x_L, which was not significant (marked with an X). (C) Diagram illustrating the findings from B. (D) Mitochondrial fission/fusion ratios were calculated from the results shown in Fig. 5 and converted to events per hour. The dotted line marks the theoretical fission/fusion ratio of 1; error bars indicate 25% and 75% bootstrapped quantiles. (E) During steady-state, the number and mass of mitochondria per cell (boxes) must remain equal. This is achieved by an unknown relationship between mitochondrial fission, fusion, biogenesis, and degradation. Parenthetic values for mitochondrial numbers are derived from fission/fusion ratios in Bcl-x_L–expressing neurons determined in D.

fission that occurs above the rate of fusion. Because mitochondrial organelles are apparently degraded by a lysosomal pathway called mitophagy (Kim et al., 2007; Kanki and Klionsky, 2008), it is reasonable to assume that organelle degradation balances the discrepancy between fission and fusion rates. For example, in neurons overexpressing Bcl-x_L, the ratio of fission/fusion is 4:1, resulting in a net gain of three mitochondria that presumably must be degraded (Fig. 6 E, left). Although mitochondrial degradation is required to conserve mitochondrial numbers, it also causes another imbalance caused by a net loss of mitochondrial mass (degradation without biogenesis). Therefore, to satisfy the conservation of mitochondrial mass at steady state, at least a portion of the mitochondrial organelles in a cell must grow in size by the exact same amount that is lost through degradation (Fig. 6 E, right).

Bcl-x_L increases mitochondrial biomass

Although Bcl-2 family proteins are not known to regulate mitochondrial biogenesis, we considered the possibility that the increase in mitochondrial length in neuronal processes was due in part to increased mitochondrial biomass induced by Bcl-x_L. Mitochondrial biomass was estimated by calculating the total mitochondrial length (sum of all mitochondria) in a given length of dendrite. This was achieved by multiplying the mean mitochondrial length (from Fig. 2 B) by the density of mitochondrial organelles in dendrites. The number density of mitochondria was determined by counting the number of organelles (marked with mtRFP) per length of dendrite (Fig. 7 A). Although dnDrp1^{K38A} modestly reduced mitochondrial number density in neuronal processes (consistent with its ability to inhibit fission), Bcl-x_L did not significantly affect the number density (Fig. 7 A). However, taking together the mitochondrial length and number density, the calculated increase in mitochondrial mass induced by Bcl-x_L is 1.4-fold. Expression of dnDrp1^{K38A} had a similar effect, and coexpression with Bcl-x_L produced an additive effect (Fig. 7 B). Therefore, in contrast to Bcl-x_L–stimulated fission, which was dependent on Drp1, the increase in mitochondrial mass by Bcl-x_L and dnDrp1^{K38A} appears to occur at least in part by independent mechanisms (Fig. 7 C).

Although predicted from Fig. 6 E, mitochondrial mass as calculated in Fig. 7 B is subject to several potential errors, including the possibilies that mitochondrial length may not

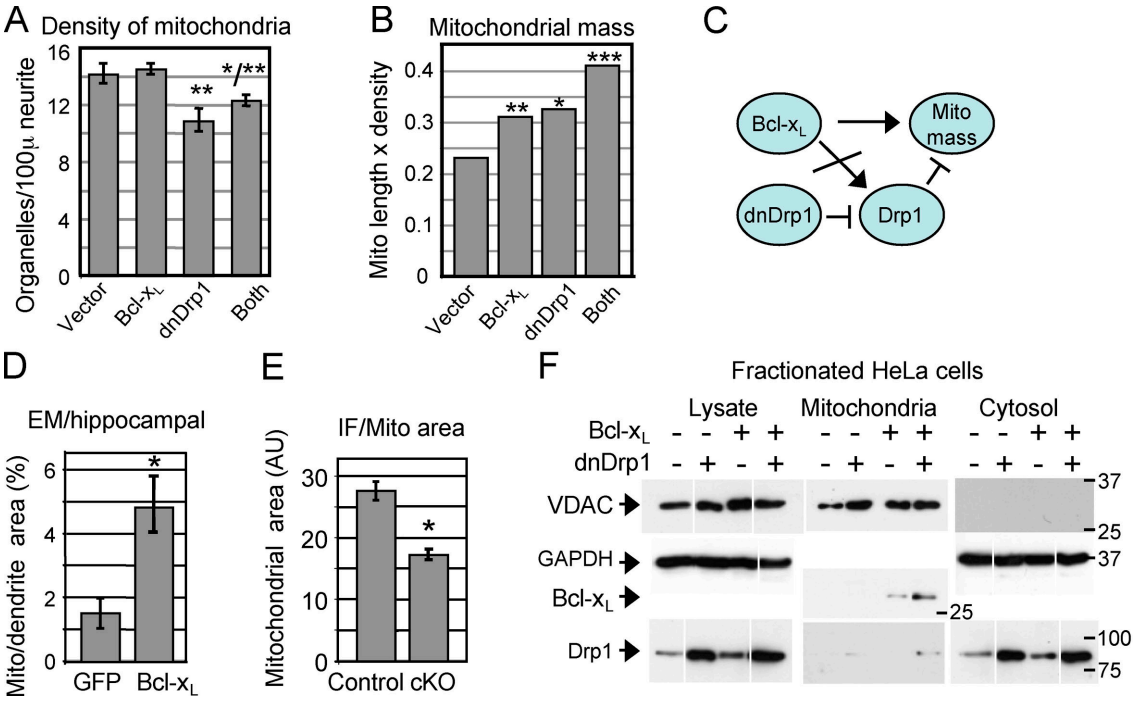

Figure 7. **Bcl-x_L promotes Drp1-independent mitochondrial growth.** (A) The number density of mitochondrial organelles was determined as the number of mitoRFP-expressing mitochondria per 100 microns of neuron process in four independent experiments per condition and presented as mean ± SEM. **, P < 0.003 compared with vector or Bcl-x_L, except vector compared to both; *, P < 0.03. See "Computational methods" and Table S2 (available at http://www.jcb.org/cgi/content/full/jcb.200809060/DC1). (B) Mitochondrial mass was approximated using the formula: [(mean mitochondrial length from Fig. 2 B) × (mitochondrial number density/micrometer from panel A)]; SEM < 0.03 for all conditions. Bootstrap significance tests were used for effective mitochondrial mass; *, P < 0.02; **, P < 0.002; ***, P = 0.0002 compared with vector control. (C) Diagram of findings from B. (D) Bcl-x_L increases the mitochondrial content of hippocampal neuronal processes determined by electron microscopy. The total area of neuronal processes that was occupied by mitochondria was calculated for at least 50 mitochondria per condition in 19 images for GFP–Bcl-x_L and in 29 images of GFP, and presented as mean ± SEM. *t* test; *, P < 0.002. (E) The area within control and *bcl-x* cKO mouse cortical neurons (6–8 DIV) that is occupied by mitochondria was determined by immunofluorescence microscopy for cytochrome *c* and analyzed using ImageJ. Neurons were identified by staining with anti-Cre (not depicted). Data are presented as mean ± SEM for 28–34 healthy neurons in 9–10 independent cultures per condition in two experiments. *t* test; *, P < 2×10^{-7}. (F) Immunoblots of lysates and indicated subcellular fractions prepared from transiently transfected HeLa cells. Some lanes from the same exposures of the same blots were rearranged for presentation. Bcl-x_L was estimated by densitometry to increase VDAC levels in mitochondrial fractions over loading control by 2.7-fold (as shown), and in two additional independent experiments by 13.0-fold and 2.3-fold. These values do not take into account <100% transfection efficiency. Molecular mass markers are shown (kD).

approximate mitochondrial mass, that mitochondria-targeted fluorescent markers are deleterious, that exogenous Bcl-x_L is not reflective of endogenous protein, that equilibrium is not reached by 24 h after transfection, or that our findings are unique to cortical neurons. To address these issues, electron microscopy was performed on 2-wk rat hippocampal neuron cultures 1 wk after efficient transduction with a lentivirus expressing either cytosolic/untargeted GFP or the GFP–Bcl-x_L fusion protein. The area within neuronal processes that was occupied by mitochondria was determined relative to the total area of neuronal processes, revealing that Bcl-x_L significantly increased the area occupied by mitochondria (Fig. 7 D). Although *bcl-x* cKO neurons are too frail for DrOF analysis, mitochondrial content was evaluated by immunofluorescence microscopy, quantifying the area occupied by mitochondria stained for cytochrome *c* (Fig. 7 E) and by immunoblot analysis for cytochrome *c* (not depicted). The *bcl-x* cKO cultures had significantly reduced mitochondrial area compared with matched controls, which is consistent with a reduction in mitochondrial content in neurons lacking Bcl-x_L.

To determine if Bcl-x_L expression leads to an elevated level of mitochondria in immortalized cells, mitochondrial content of transiently transfected HeLa cells was analyzed by comparing relative levels of voltage-dependent anion channel (VDAC), an abundant outer mitochondrial membrane protein. Bcl-x_L and dnDrp1^{K38A} clearly increased VDAC levels relative to glyceraldehyde 3-phosphate dehydrogenase (or actin in some experiments; not depicted) despite <100% transfection efficiency (Fig. 7 F). The expression of transfected dnDrp1^{K38A} and Bcl-x_L was confirmed as expected and correlated with increased mitochondrial content. Bcl-x_L may contribute to enhanced neuronal function and to cell survival in general by increasing mitochondrial capacity.

Discussion

Bcl-2 family members are best known as regulators of mitochondria-mediated apoptotic events that occur within an hour before cell death. However, as supported by the work described in this paper, Bcl-2 proteins may have additional mitochondrial functions in healthy, long-lived cells. We took advantage of the linear (one-dimensional) topology of neuronal processes to directly assess the effects of mitochondrial fission and fusion on

mitochondrial morphology in healthy neurons. Although these results generally agree with results from indirect methods and morphology studies suggesting that Bcl-x_L can increase either fusion or fission of mitochondria, quantification of fission and fusion rates revealed unexpectedly that fission exceeds fusion with or without Bcl-x_L by up to sixfold, with fusion occurring in only 16% of mitochondria per hour. Therefore, other parameters that include mitochondrial biogenesis and degradation must be invoked to compensate for this fission/fusion imbalance to maintain mitochondrial number at steady state. These studies also suggest that Bcl-x_L may affect mitochondrial shape through regulating mitochondrial biomass independently of fission–fusion mechanisms.

The terms fission and fusion are often used to describe morphologies rather than the underlying processes of organelle fission and fusion. This study predicts that a fission/fragmented mitochondrial phenotype does not equate with a higher fission/fragmentation rate, or even a lower fusion rate, because a lower growth/elongation rate could potentially be the responsible parameter. In our case, paradoxically, longer mitochondria are observed even when the fission rate is increased by Bcl-x_L (e.g., Figs. 2 and 5). Furthermore, it is conceivable that cells with opposite mitochondrial morphologies (connected vs. fragmented) could both have higher total mitochondrial mass/content. For example, although Bcl-x_L can increase mitochondrial content of cells under conditions where the mitochondria are elongated (see Figs. 2 and 7), Bcl-x_L may also increase mitochondrial content under conditions where Bcl-x_L induces a more fragmented morphology (at least in the axons; Li et al., 2008). In addition, mitochondrial fragmentation can correlate with cell death resistance or sensitivity (Parone et al., 2006; Norris and Youle, 2008; Sheridan et al., 2008). Although mitochondrial morphology changes may be separable from cell death mechanisms, we venture that they are related, but that their relationships are not yet clear.

Integrating mitochondrial fission, fusion, biogenesis, and degradation

By definition, if Bcl-x_L increases biogenesis of mitochondrial organelles, as suggested by these studies, there must be a compensatory increase in mitochondrial degradation to maintain the newly established steady-state levels in neurons and other cell types expressing Bcl-x_L (thereby preventing eventual filling of the entire cell with mitochondria; see Fig. 6 E). Perhaps this compensatory degradation is also facilitated by Bcl-x_L–induced Drp1-dependent fission based on the observation by others that a mitochondrial fission event can lead to depolarization and degradation of one of the two daughter mitochondria (Twig et al., 2008). Theoretically, we would expect to observe mitochondrial degradation in neuronal processes during the time-lapse studies based on our predicted rates of degradation, but this was not the case. A possible explanation is that mitochondria may be transported back toward the cell body or elsewhere for degradation. Alternatively, we missed these events after fission because one of two daughter mitochondria often migrated out of the field within 15 min, as newly generated mitochondria were often transported more rapidly away from a less mobile "parent" mitochondrion, irrespective of Bcl-x_L status.

An alternative explanation for increased biomass with Bcl-x_L is inhibition of mitochondrial degradation. Mitophagy could be inhibited by Bcl-x_L through an interaction with Beclin (Pattingre et al., 2005; Maiuri et al., 2007), though we did not observe an increase in mitochondrial numbers in neuronal processes with Bcl-x_L (Fig. 7 A). Even if Bcl-x_L is a direct inhibitor of mitochondrial degradation, eventually this must be compensated by a matched decline in biogenesis to satisfy steady-state conditions (Fig. 6 E). This decline in the normal turnover (potentially of damaged organelles), plus the compensatory decline in biogenesis, seems unlikely to explain the beneficial effects of Bcl-x_L in neurons. However, a reduced turnover of healthy mitochondria could also conserve energy. Like many dynamic cellular processes, there are likely to be regulatory feedback mechanisms at each control point (fission, fusion, biogenesis, and degradation) to compensate for imbalances in the system. As a consequence, it is challenging to dissect the underlying cause of any disturbance to the balance, as perturbation of any one parameter will trigger adjustments to one or more of the other parameters followed by reestablishment of new steady-state conditions. Furthermore, it remains possible that Bcl-x_L could modulate the balance of these parameters in either direction depending on metabolic needs.

Although dnDrp1^{K38A} inhibited mitochondrial fission as expected (Fig. 6 B), it unexpectedly also increased the fusion rate, similar to Bcl-x_L (Fig. 5, B and C). If we assume that Drp1 does not directly mediate fusion (supported by yeast genetics), then we must invoke indirect effects to explain this observation. Drp1 is predominantly cytosolic, and a fraction of Drp1 cycles on and off mitochondria (Smirnova et al., 1998), presumably to maintain steady-state fission rates. Drp1 recruitment to mitochondria is increased under certain conditions, such as after an apoptotic stimulus (Frank et al., 2001). Interestingly, Drp1 has been shown to cocluster at mitochondrial fission sites with the mitochondrial fusion protein Mfn2, at least at the resolution of microscopy (Karbowski et al., 2002). Thus, dnDrp1^{K38A} could conceivably interfere with the ability of endogenous Drp1 to compete with Mfn2 at shared docking points, thereby removing restrictions on Mfn2-mediated fusion. In an alternative scheme, faster mitochondrial transport would increase the number of times mitochondria encounter one another, and if the rate of encounters is proportional to the rate of fusion, then dnDrp1^{K38A} (or Bcl-x_L) could potentially increase fusion by increasing rates of transport. However, we did not detect significant differences in the proportion of stationary mitochondria, or the proportion of mitochondria undergoing fast transport (> 0.5 µm/s) with dnDrp1^{K38A} and/or Bcl-x_L (unpublished data). Bcl-x_L has also been reported to interact with Mfn2 independently of Drp1 by coimmunoprecipitation and, therefore, Bcl-x_L may directly stimulate mitochondrial fusion (Delivani et al., 2006).

Evaluating mitochondrial dynamics and their physiological consequences

It is difficult to directly compare the rates of mitochondrial fission and fusion events to published methods that measure fluorescence diffusion. With this caveat, our fusion rates appear to be much lower than those reported in HeLa cells, and perhaps

even lower than the slow rates observed in primary hippocampal neurons (Karbowski et al., 2004). Nevertheless, others have found lower rates in postmitotic cells compared with their proliferating counterparts (Jendrach et al., 2005). However, we only rarely observed coupling between mitochondrial fusion and fission, in contrast to results in COS7 and INS1 cells, where a fission event frequently occurred within 100 s after a fusion event (Twig et al., 2008).

Mitochondrial morphology changes have long been associated with energetic status, but the mechanistic connections between mitochondrial energetics and mitochondrial morphology remain unclarified (Benard and Rossignol, 2008). Depletion or inhibition of Drp1 was found to impair respiratory capacity (Twig et al., 2008), to cause a depletion of mitochondria from nerve terminals in *Drosophila melanogaster* (Verstreken et al., 2005), and to reduce the number of synapses and dendritic spines in cultured mammalian neurons (Li et al., 2004; Li et al., 2008).

It is conceivable that the effects of Bcl-x_L on mitochondria in healthy cells also contribute to its potent anti-death activity by fortifying the energetic capacity of both dividing and nondividing cells, thereby improving the chances of cell survival upon receiving a toxic insult or apoptotic death stimulus. Although we cannot rule out an indirect effect of Bcl-x_L on mitochondrial dynamics that stems from an underlying primary effect on energetics, a direct role for Bcl-x_L is supported by several studies of Bcl-2 family proteins interacting with mitochondrial dynamin-like fission and fusion factors (Delivani et al., 2006; Brooks et al., 2007; Li et al., 2008). These effects of Bcl-x_L on mitochondrial shape could also involve binding and inhibiting pro-death Bcl-2 family proteins such as Bax and Bak, though Bcl-x_L apparently has Bax/Bak-independent pro-survival activities based on Bax/Bak nonbinding mutants of Bcl-x_L that retain pro-survival function (Cheng et al., 1996). Conversely, because Bax and Bcl-x_L both increase mitochondrial length in healthy cells, it is also possible that they act cooperatively to alter one or more of the parameters that regulate steady-state mitochondrial shape.

Because mitochondria are apparently not synthesized de novo, mitochondrial fission is necessary for production of new mitochondria. Bcl-x_L increases Drp1-mediated fission and increases synapse formation in both axons and dendrites of cultured neurons (Hickman et al., 2008; Li et al., 2008). These functions may explain in part why Bcl-x_L is required for neuronal survival during brain development (Motoyama et al., 1995). Many neurodegenerative disorders may begin at neuron terminals, and dynamic synaptic changes can occur in the absence of cell body input (Wishart et al., 2006; Bettini et al., 2007), raising the possibility that Bcl-x_L will be a determinant in neurodegeneration.

Materials and methods

bcl-x cKO mouse

Floxed *bcl-x* mice (Wagner et al., 2000) were bred with NEX-CRE knockin mice (Goebbels et al., 2006) to generate conditional *bcl-x* knockout (*bcl-x*$^{flox/flox}$;*nex*$^{cre/+}$) and control embryos (*bcl-x*$^{flox/+}$;*nex*$^{cre/+}$). cKO mice are born at near normal ratios. All animal procedures were approved by the Animal Care and Use Committee.

Primary cortical neurons

Cortical neuron cultures were prepared from individual E16.5 *bcl-x* cKO and control mouse embryos, and from pooled E18 rat cortices, using a modified method from Ghosh and Greenberg (1995). In brief, cortices were dissected separately in HBSS on ice, digested with 8 U/ml (mouse) or 20 U/ml (rat) papain (Worthington Biochemical Corporation) for 20 min, treated with a trypsin inhibitor (Sigma-Aldrich), washed, and dissociated by titration with a pipet. Mouse neurons from individual embryos were plated on glass coverslips coated with 10 µg/ml poly-L-ornithine (Sigma-Aldrich) in neurobasal medium (Invitrogen) plus 2% glutamax and 2% B27 supplement (Invitrogen) at two different densities (4.5×10^5 and 7.5×10^5 cells/ml per 35-mm dish) to compensate for spontaneous death of *bcl-x* cKO, and maintained by replacing 50% of the medium every 3 d. Culture genotypes were determined by PCR as described previously (Wagner et al., 2000; Goebbels et al., 2006), and paired control and *bcl-x* cKO cultures of similar cell densities were used for experiments. Rat neurons were plated at 3×10^5/ml on glass-bottom dishes precoated with poly-L-lysine (MatTek) in the same medium except with penicillin/streptomycin and 5% fetal calf serum, and the medium was replaced after 3 h. Rat and mouse cultures were maintained with 50% medium changes every 3 d.

Plasmids and transfections

Cortical neuron culture medium was removed, stored at 37°C, and replaced with transfection medium (MEM, pH 7.4, 2% glutamax, 20 mM Hepes, 33 mM glucose, and 1 mM sodium-pyruvate). Plasmids expressing mtRFP, photoactivatable GFP targeted to mitochondria via sequences from cytochrome *c* oxidase subunit VIII (mtPA-GFP; provided by R. Youle, National Institute of Neurological Disease and Stroke at the National Institutes of Health, Bethesda, MD), full-length human Bcl-x_L, a dominant-interfering K38A mutant of human Drp1 (Smirnova et al., 1998; Labrousse et al., 1999), or empty vector (pDB59) were transfected into 7-d cortical cultures. A total of 4 µg of DNA plasmids (1 µg per expression construct, 0–1 µg of empty vector per 4.5×10^5 neurons per dish) was preincubated in 250 µl Optimem (Invitrogen) and combined with 5 µl Lipofectamine 2000 (Invitrogen). Transfection mixes were incubated with cells at 37°C without CO_2 for 2 h and replaced with stored medium. Low-density cultures of HeLa cells were transfected with Lipofectamine 2000 according to the manufacturer's instructions and harvested 24 h after transfection. This protocol was applied to all experiments shown in Figs. 2–6 and Fig. 7, A–C.

Immunocytochemistry and immunoblot analyses

Cortical neuron cultures were washed with Lock's buffer (154 mM NaCl, 5.6 mM KCl, 2.3 mM $CaCl_2$, 1.0 mM $MgCl_2$, 5 mM Hepes, and 10 mM glucose, pH 7.4), fixed for 15 min in 4% paraformaldehyde, permeabilized with 0.2% Triton X-100 for 5 min, and blocked with 5% normal goat serum at RT for 30 min. Cells were incubated at 4°C overnight with primary antibodies: rabbit anti–Bcl-$x_{L/S}$ antibody (1:1,000; BioCarta), rabbit anti-Cre (1:2,000), or mouse anti–cytochrome *c* (1:80; BD). Secondary antibodies goat anti–mouse Alexa Fluor 488 (Invitrogen) and goat anti–rabbit Cy3 (Jackson ImmunoResearch Laboratories) were applied at RT for 1 h. Fluorescent images were captured with a Spot RT camera (Diagnostic Instruments, Inc.) and an Eclipse E800 microscope (40× objective; Nikon) and analyzed using ImageJ. Immunoblots were probed with rabbit anti–Bcl-x polyclonal antibody (1:2,000; provided by Larry Boise, University of Miami, Miami, FL), anti-porin/VDAC monoclonal antibody 31HL (1:2,000; Invitrogen), anti–glyceraldehyde 3-phosphate dehydrogenase monoclonal antibody 6C5 (1:1,000; Santa Cruz Biotechnology, Inc.), anti-Drp1 (1:1000; BD), or anti-actin monoclonal clone C4 (1:2,000; MP Biomedicals).

Mitochondrial length of mouse neurons

Mouse cortical neuron cultures were fixed in 4% paraformaldehyde 1 d after transfection and imaged with an inverted microscope (TE200; Nikon) at 100× magnification, and images were captured with a Spot RT camera. Morphological measurements were made using Simple PCI software (Hamamatsu) in a blinded fashion by automated object identification with user-defined thresholds for pixel intensity and size. Objects are skeletonized and measurements of length were obtained.

Mitochondrial length and DrOF in rat neurons

All live-cell imaging was performed 1 d after transfection in a 37°C chamber using a confocal microscope (LSM510 Meta; Carl Zeiss, Inc.) and LSM 510 software version 3.2 (60× oil immersion objective lens; Nikon). For all studies, 2–4 fields per dish and duplicate dishes per condition were evaluated in each of eight independent experiments. For imaging, cortical culture medium was replaced with equal volume of warmed medium. Fields containing neurites expressing mtRFP were identified, and several minimal regions

per field, each containing a single randomly selected mitochondrion, were photoactivated with a 405-nm laser line at 1.9 mW and a 4.8-ms total pixel time to activate cotransfected mtPA-GFP (Fig. 3). Time-lapse imaging was initiated immediately, and images were acquired every 10 s for 15 min (90 images) by excitation at 488 and 543 nm. Use of a scanning light source and short observation period minimized photodamage and prevented nonspecific activation of photoactivatable GFP. Mitochondrial fusion and fission events were quantified by manual review of captured images with encrypted identities using the LSM browser software (Carl Zeiss, Inc.). Apparent fission events that occurred within the first two images (10 s) were not scored to avoid false events because of simultaneous activation of a second passing mitochondrion. Length and number of mitochondria and length of neuronal processes were calculated using ImageJ software at the 0 time point from the live imaging series. There was no evidence of phototoxicity, as no changes in rates of axonal mitochondrial transport were detected after photoactivation, and maximal transport rates were similar to reported rates (Hollenbeck, 1996; Ligon and Steward, 2000). Activation of mtPA-GFP was reported not to alter mitochondrial membrane potential and to be insensitive to changes in mitochondrial membrane potential (Twig et al., 2006).

Electron microscopy

Hippocampal neuron cultures (13–14 DIV) prepared from E18 embryonic rats were transduced with lentiviruses expressing GFP or GFP–hBcl-x_L fusion protein to achieve gene expression in ~100% of the neurons (Li et al., 2008). At 7 d after infection, cultures were prepared for electron microscopy as described previously (Li et al., 2008). 50 micrographs from each condition were analyzed by determining the area of each neurite and the fraction of this area that was occupied by mitochondria using Adobe Photoshop (pixels squared).

Computational methods

All statistical analyses and numerical computations were performed by scripts written in the R statistical analysis system.

Significance tests. Binomial tests were used throughout to test the null hypothesis that two proportions are the same. Bonferroni-corrected threshold p-values are used to determine whether p-values are significant in multiple comparisons.

Inferring the fission rate per unit length (*p*) from the observed proportion of nonfissioning mitochondria and the mitochondrial length distribution. Consider a population of N mitochondria. Let p_i be the probability that the i^{th} mitochondrion does not fission. Then, the expected number of mitochondria that do not fission is:

$$E\{N-m\} = \sum_{i=1}^{N} p_i \quad (1),$$

where m is the number of mitochondria that do fission. To obtain p_i, assume that fissions are equally likely to occur at any time and anywhere along the length s_i of the i^{th} mitochondrion. Under this assumption, the probability of observing exactly k fission events in a time T in a single mitochondrion is Poisson distributed. Thus, because p is the fission probability per unit time per unit mitochondrial length, it follows that the probability that a fission event does not occur in time T in the i^{th} mitochondrion is:

$$p_i = \exp\left(-pTs_i\right) \quad (2).$$

Substituting Eq. 2 into Eq. 1 and dividing both sides by N yields an expression for the expected fraction of mitochondria that do not fission:

$$E\left\{\frac{N-m}{N}\right\} = \frac{1}{N}\sum_{i=1}^{N}\exp\left(-pTs_i\right) \quad (3).$$

More generally, we note that the mean on the right-hand side of Eq. 3 need not be performed over the same mitochondria used on the left-hand side (Eq. 3); thus, we can relate the measurements of mitochondrial lengths to the measurements of fission events, provided that the mitochondria used in the two measurements are drawn from the same population. Under this assumption, we finally obtain:

$$E\left\{\frac{N-m}{N}\right\} = \frac{1}{K}\sum_{i=1}^{K}\exp\left(-pTs_i\right) \quad (4),$$

where K is the number of mitochondria whose lengths are measured and N is the number mitochondrion that are activated and monitored for fission events. This nonlinear equation can be solved for p using numerical methods, or it can be solved analytically under various approximations. Approximate solutions and numerical solutions are compared in the online supplemental material.

The standard error of the numerically calculated values of p are estimated by bootstrapping the solution of Eq. 4; i.e., we resample the length distribution with replacement and then resolve Eq. 4 for p using this resampled distribution of lengths. 1,000 bootstrap samples were used for all bootstrap calculations. The standard deviation of the resulting 1,000 solved p's is the reported standard error in the estimated p.

Online supplemental material

Table S1 shows summary statistics of the raw data used for DrOF results in Figs. 2 and 5–7. Table S2 compares the exact (numerical) solutions of Eq. 4 to various approximate solutions. Video 1 shows a 15-min time-lapse series (10 s/frame) of mitochondria moving through processes of primary rat cortical neurons that coexpress mtRFP and mtPA-GFP (see DrOF methods and Fig. 3). Video 2 shows a photoactivated mitochondrion undergoing two fission events (see Video 1 legend and Fig. 3 B). Video 3 shows a photoactivated mitochondrion undergoing fusion with another mitochondrion (see Video 1 legend). Video 4 shows a photoactivated and an unactivated mitochondrion undergoing fusion (see Video 1 legend and Fig. 3 C). Online supplemental material is available at http://www.jcb.org/cgi/content/full/jcb.200809060/DC1.

We thank Shifa Zou and Marc Pypaert for technical expertise.

This work was supported by National Institutes of Health grants NS037402 and NS034175 (to J.M. Hardwick), KO8 NS059576 (to S.B. Berman), and NS045876 (to E.A. Jonas).

Submitted: 10 September 2008
Accepted: 22 January 2009

References

Adams, J.M., and S. Cory. 2007. Bcl-2-regulated apoptosis: mechanism and therapeutic potential. *Curr. Opin. Immunol.* 19:488–496.

Amiri, M., and P.J. Hollenbeck. 2008. Mitochondrial biogenesis in the axons of vertebrate peripheral neurons. *Dev. Neurobiol.* 68:1348–1361.

Barsoum, M.J., H. Yuan, A.A. Gerencser, G. Liot, Y. Kushnareva, S. Graber, I. Kovacs, W.D. Lee, J. Waggoner, J. Cui, et al. 2006. Nitric oxide-induced mitochondrial fission is regulated by dynamin-related GTPases in neurons. *EMBO J.* 25:3900–3911.

Basanez, G., and J.M. Hardwick. 2008. Unravelling the bcl-2 apoptosis code with a simple model system. *PLoS Biol.* 6:e154.

Benard, G., and R. Rossignol. 2008. Ultrastructure of the mitochondrion and its bearing on function and bioenergetics. *Antioxid. Redox Signal.* 10:1313–1342.

Berman, S.B., F.J. Pineda, and J.M. Hardwick. 2008. Mitochondrial fission and fusion dynamics: the long and short of it. *Cell Death Differ.* 15:1147–1152.

Bettini, N.L., T.S. Moores, B. Baxter, J. Deuchars, and S.H. Parson. 2007. Dynamic remodelling of synapses can occur in the absence of the parent cell body. *BMC Neurosci.* 8:79.

Bhar, D., M.A. Karren, M. Babst, and J.M. Shaw. 2006. Dimeric Dnm1-G385D interacts with Mdv1 on mitochondria and can be stimulated to assemble into fission complexes containing Mdv1 and Fis1. *J. Biol. Chem.* 281:17312–17320.

Boldogh, I.R., and L.A. Pon. 2007. Mitochondria on the move. *Trends Cell Biol.* 17:502–510.

Breckenridge, D.G., M. Stojanovic, R.C. Marcellus, and G.C. Shore. 2003. Caspase cleavage product of BAP31 induces mitochondrial fission through endoplasmic reticulum calcium signals, enhancing cytochrome c release to the cytosol. *J. Cell Biol.* 160:1115–1127.

Bredesen, D.E. 2008. Programmed cell death mechanisms in neurological disease. *Curr. Mol. Med.* 8:173–186.

Brooks, C., Q. Wei, L. Feng, G. Dong, Y. Tao, L. Mei, Z.J. Xie, and Z. Dong. 2007. Bak regulates mitochondrial morphology and pathology during apoptosis by interacting with mitofusins. *Proc. Natl. Acad. Sci. USA.* 104:11649–11654.

Cassidy-Stone, A., J.E. Chipuk, E. Ingerman, C. Song, C. Yoo, T. Kuwana, M.J. Kurth, J.T. Shaw, J.E. Hinshaw, D.R. Green, and J. Nunnari. 2008. Chemical inhibition of the mitochondrial division dynamin reveals its

role in Bax/Bak-dependent mitochondrial outer membrane permeabilization. *Dev. Cell.* 14:193–204.

Cerveny, K.L., Y. Tamura, Z. Zhang, R.E. Jensen, and H. Sesaki. 2007. Regulation of mitochondrial fusion and division. *Trends Cell Biol.* 17:563–569.

Chan, D.C. 2006. Mitochondria: dynamic organelles in disease, aging, and development. *Cell.* 125:1241–1252.

Cheng, E.H., B. Levine, L.H. Boise, C.B. Thompson, and J.M. Hardwick. 1996. Bax-independent inhibition of apoptosis by Bcl-XL. *Nature.* 379:554–556.

Chipuk, J.E., and D.R. Green. 2008. How do BCL-2 proteins induce mitochondrial outer membrane permeabilization? *Trends Cell Biol.* 18:157–164.

Chung, K.W., S.Y. Cho, S.J. Hwang, K.H. Kim, J.H. Yoo, O. Kwon, S.M. Kim, I.N. Sunwoo, S. Zuchner, and B.O. Choi. 2008. Early-onset stroke associated with a mutation in mitofusin 2. *Neurology.* 70:2010–2011.

Delivani, P., C. Adrain, R.C. Taylor, P.J. Duriez, and S.J. Martin. 2006. Role for CED-9 and Egl-1 as regulators of mitochondrial fission and fusion dynamics. *Mol. Cell.* 21:761–773.

Detmer, S.A., and D.C. Chan. 2007. Functions and dysfunctions of mitochondrial dynamics. *Nat. Rev. Mol. Cell Biol.* 8:870–879.

Dimauro, S., and E.A. Schon. 2008. Mitochondrial disorders in the nervous system. *Annu. Rev. Neurosci.* 31:91–123.

Escobar-Henriques, M., B. Westermann, and T. Langer. 2006. Regulation of mitochondrial fusion by the F-box protein Mdm30 involves proteasome-independent turnover of Fzo1. *J. Cell Biol.* 173:645–650.

Fannjiang, Y., C.H. Kim, R.L. Huganir, S. Zou, T. Lindsten, C.B. Thompson, T. Mito, R.J. Traystman, T. Larsen, D.E. Griffin, et al. 2003. BAK alters neuronal excitability and can switch from anti- to pro-death function during postnatal development. *Dev. Cell.* 4:575–585.

Fannjiang, Y., W.C. Cheng, S.J. Lee, B. Qi, J. Pevsner, J.M. McCaffery, R.B. Hill, G. Basanez, and J.M. Hardwick. 2004. Mitochondrial fission proteins regulate programmed cell death in yeast. *Genes Dev.* 18:2785–2797.

Frank, S. 2006. Dysregulation of mitochondrial fusion and fission: an emerging concept in neurodegeneration. *Acta Neuropathol.* 111:93–100.

Frank, S., B. Gaume, E.S. Bergmann-Leitner, W.W. Leitner, E.G. Robert, F. Catez, C.L. Smith, and R.J. Youle. 2001. The role of dynamin-related protein 1, a mediator of mitochondrial fission, in apoptosis. *Dev. Cell.* 1:515–525.

Gandre-Babbe, S., and A.M. van der Bliek. 2008. The novel tail-anchored membrane protein Mff controls mitochondrial and peroxisomal fission in mammalian cells. *Mol. Biol. Cell.* 19:2402–2412.

Ghosh, A., and M.E. Greenberg. 1995. Distinct roles for bFGF and NT-3 in the regulation of cortical neurogenesis. *Neuron.* 15:89–103.

Goebbels, S., I. Bormuth, U. Bode, O. Hermanson, M.H. Schwab, and K.A. Nave. 2006. Genetic targeting of principal neurons in neocortex and hippocampus of NEX-Cre mice. *Genesis.* 44:611–621.

Goyal, G., B. Fell, A. Sarin, R.J. Youle, and V. Sriram. 2007. Role of mitochondrial remodeling in programmed cell death in *Drosophila melanogaster*. *Dev. Cell.* 12:807–816.

Hickman, J.A., J.M. Hardwick, L.K. Kaczmarek, and E.A. Jonas. 2008. Bcl-xL inhibitor ABT-737 reveals a dual role for Bcl-xL in synaptic transmission. *J. Neurophysiol.* 99:1515–1522.

Hollenbeck, P.J. 1996. The pattern and mechanism of mitochondrial transport in axons. *Front. Biosci.* 1:d91–d102.

Hoppins, S., L. Lackner, and J. Nunnari. 2007. The machines that divide and fuse mitochondria. *Annu. Rev. Biochem.* 76:751–780.

Jagasia, R., P. Grote, B. Westermann, and B. Conradt. 2005. DRP-1-mediated mitochondrial fragmentation during EGL-1-induced cell death in *C. elegans*. *Nature.* 433:754–760.

James, D.I., P.A. Parone, Y. Mattenberger, and J.C. Martinou. 2003. hFis1, a novel component of the mammalian mitochondrial fission machinery. *J. Biol. Chem.* 278:36373–36379.

Jendrach, M., S. Pohl, M. Voth, A. Kowald, P. Hammerstein, and J. Bereiter-Hahn. 2005. Morpho-dynamic changes of mitochondria during ageing of human endothelial cells. *Mech. Ageing Dev.* 126:813–821.

Jonas, E.A., D. Hoit, J.A. Hickman, T.A. Brandt, B.M. Polster, Y. Fannjiang, E. McCarthy, M.K. Montanez, J.M. Hardwick, and L.K. Kaczmarek. 2003. Modulation of synaptic transmission by the BCL-2 family protein BCL-xL. *J. Neurosci.* 23:8423–8431.

Kanki, T., and D.J. Klionsky. 2008. Mitophagy in yeast occurs through a selective mechanism. *J. Biol. Chem.* 283:32386–32393.

Karbowski, M., Y.J. Lee, B. Gaume, S.Y. Jeong, S. Frank, A. Nechushtan, A. Santel, M. Fuller, C.L. Smith, and R.J. Youle. 2002. Spatial and temporal association of Bax with mitochondrial fission sites, Drp1, and Mfn2 during apoptosis. *J. Cell Biol.* 159:931–938.

Karbowski, M., D. Arnoult, H. Chen, D.C. Chan, C.L. Smith, and R.J. Youle. 2004. Quantitation of mitochondrial dynamics by photolabeling of individual organelles shows that mitochondrial fusion is blocked during the Bax activation phase of apoptosis. *J. Cell Biol.* 164:493–499.

Karbowski, M., K.L. Norris, M.M. Cleland, S.Y. Jeong, and R.J. Youle. 2006. Role of Bax and Bak in mitochondrial morphogenesis. *Nature.* 443:658–662.

Kim, I., S. Rodriguez-Enriquez, and J.J. Lemasters. 2007. Selective degradation of mitochondria by mitophagy. *Arch. Biochem. Biophys.* 462:245–253.

Knott, A.B., G. Perkins, R. Schwarzenbacher, and E. Bossy-Wetzel. 2008. Mitochondrial fragmentation in neurodegeneration. *Nat. Rev. Neurosci.* 9:505–518.

Krajewski, S., M. Krajewska, A. Shabaik, H.G. Wang, S. Irie, L. Fong, and J.C. Reed. 1994. Immunohistochemical analysis of in vivo patterns of Bcl-X expression. *Cancer Res.* 54:5501–5507.

Labrousse, A.M., M.D. Zappaterra, D.A. Rube, and A.M. van der Bliek. 1999. *C. elegans* dynamin-related protein DRP-1 controls severing of the mitochondrial outer membrane. *Mol. Cell.* 4:815–826.

Lewis, J., G.A. Oyler, K. Ueno, Y.R. Fannjiang, B.N. Chau, J. Vornov, S.J. Korsmeyer, S. Zou, and J.M. Hardwick. 1999. Inhibition of virus-induced neuronal apoptosis by Bax. *Nat. Med.* 5:832–835.

Li, H., Y. Chen, A.F. Jones, R.H. Sanger, L.P. Collis, R. Flannery, E.C. McNay, T. Yu, R. Schwarzenbacher, B. Bossy, et al. 2008. Bcl-xL induces Drp1-dependent synapse formation in cultured hippocampal neurons. *Proc. Natl. Acad. Sci. USA.* 105:2169–2174.

Li, Z., K. Okamoto, Y. Hayashi, and M. Sheng. 2004. The importance of dendritic mitochondria in the morphogenesis and plasticity of spines and synapses. *Cell.* 119:873–887.

Ligon, L.A., and O. Steward. 2000. Movement of mitochondria in the axons and dendrites of cultured hippocampal neurons. *J. Comp. Neurol.* 427:340–350.

Maiuri, M.C., A. Criollo, E. Tasdemir, J.M. Vicencio, N. Tajeddine, J.A. Hickman, O. Geneste, and G. Kroemer. 2007. BH3-only proteins and BH3 mimetics induce autophagy by competitively disrupting the interaction between Beclin 1 and Bcl-2/Bcl-X(L). *Autophagy.* 3:374–376.

Motoyama, N., F. Wang, K.A. Roth, H. Sawa, K. Nakayama, K. Nakayama, I. Negishi, S. Senju, Q. Zhang, S. Fujii, et al. 1995. Massive cell death of immature hematopoietic cells and neurons in Bcl-x-deficient mice. *Science.* 267:1506–1510.

Mozdy, A.D., J.M. McCaffery, and J.M. Shaw. 2000. Dnm1p GTPase-mediated mitochondrial fission is a multi-step process requiring the novel integral membrane component Fis1p. *J. Cell Biol.* 151:367–380.

Nicholls, D.G., and S.J. Ferguson. 2002. Bioenergetics 3. Academic Press Ltd., London. 297 pp.

Norris, K.L., and R.J. Youle. 2008. Cytomegalovirus proteins vMIA and m38.5 link mitochondrial morphogenesis to Bcl-2 family proteins. *J. Virol.* 82:6232–6243.

Okamoto, K., and J.M. Shaw. 2005. Mitochondrial morphology and dynamics in yeast and multicellular eukaryotes. *Annu. Rev. Genet.* 39:503–536.

Parone, P.A., D.I. James, S. Da Cruz, Y. Mattenberger, O. Donze, F. Barja, and J.C. Martinou. 2006. Inhibiting the mitochondrial fission machinery does not prevent Bax/Bak-dependent apoptosis. *Mol. Cell. Biol.* 26:7397–7408.

Patterson, G.H., and J. Lippincott-Schwartz. 2002. A photoactivatable GFP for selective photolabeling of proteins and cells. *Science.* 297:1873–1877.

Pattingre, S., A. Tassa, X. Qu, R. Garuti, X.H. Liang, N. Mizushima, M. Packer, M.D. Schneider, and B. Levine. 2005. Bcl-2 antiapoptotic proteins inhibit Beclin 1-dependent autophagy. *Cell.* 122:927–939.

Schauss, A.C., J. Bewersdorf, and S. Jakobs. 2006. Fis1p and Caf4p, but not Mdv1p, determine the polar localization of Dnm1p clusters on the mitochondrial surface. *J. Cell Sci.* 119:3098–3106.

Shaham, S., and H.R. Horvitz. 1996. Developing *Caenorhabditis elegans* neurons may contain both cell-death protective and killer activities. *Genes Dev.* 10:578–591.

Shaw, J.M., and J. Nunnari. 2002. Mitochondrial dynamics and division in budding yeast. *Trends Cell Biol.* 12:178–184.

Sheridan, C., P. Delivani, S.P. Cullen, and S.J. Martin. 2008. Bax- or Bak-induced mitochondrial fission can be uncoupled from cytochrome C release. *Mol. Cell.* 31:570–585.

Smirnova, E., D.L. Shurland, S.N. Ryazantsev, and A.M. van der Bliek. 1998. A human dynamin-related protein controls the distribution of mitochondria. *J. Cell Biol.* 143:351–358.

Tan, F.J., M. Husain, C.M. Manlandro, M. Koppenol, A.Z. Fire, and R.B. Hill. 2008. CED-9 and mitochondrial homeostasis in *C. elegans* muscle. *J. Cell Sci.* 121:3373–3382.

Twig, G., S.A. Graf, J.D. Wikstrom, H. Mohamed, S.E. Haigh, A. Elorza, M. Deutsch, N. Zurgil, N. Reynolds, and O.S. Shirihai. 2006. Tagging and tracking individual networks within a complex mitochondrial web with photoactivatable GFP. *Am. J. Physiol. Cell Physiol.* 291:C176–C184.

Twig, G., A. Elorza, A.J. Molina, H. Mohamed, J.D. Wikstrom, G. Walzer, L. Stiles, S.E. Haigh, S. Katz, G. Las, et al. 2008. Fission and selective fusion govern segregation and elimination by autophagy. *EMBO J.* 27:433–446.

Verstreken, P., C.V. Ly, K.J. Venken, T.W. Koh, Y. Zhou, and H.J. Bellen. 2005. Synaptic mitochondria are critical for mobilization of reserve pool vesicles at *Drosophila* neuromuscular junctions. *Neuron.* 47:365–378.

Wagner, K.U., E. Claudio, E.B. Rucker III, G. Riedlinger, C. Broussard, P.L. Schwartzberg, U. Siebenlist, and L. Hennighausen. 2000. Conditional deletion of the Bcl-x gene from erythroid cells results in hemolytic anemia and profound splenomegaly. *Development.* 127:4949–4958.

Wallace, D.C. 1999. Mitochondrial diseases in man and mouse. *Science.* 283:1482–1488.

Waterham, H.R., J. Koster, C.W. van Roermund, P.A. Mooyer, R.J. Wanders, and J.V. Leonard. 2007. A lethal defect of mitochondrial and peroxisomal fission. *N. Engl. J. Med.* 356:1736–1741.

Wishart, T.M., S.H. Parson, and T.H. Gillingwater. 2006. Synaptic vulnerability in neurodegenerative disease. *J. Neuropathol. Exp. Neurol.* 65:733–739.

Yoon, Y., E.W. Krueger, B.J. Oswald, and M.A. McNiven. 2003. The mitochondrial protein hFis1 regulates mitochondrial fission in mammalian cells through an interaction with the dynamin-like protein DLP1. *Mol. Cell. Biol.* 23:5409–5420.

Youle, R.J., and M. Karbowski. 2005. Mitochondrial fission in apoptosis. *Nat. Rev. Mol. Cell Biol.* 6:657–663.

Zuchner, S., I.V. Mersiyanova, M. Muglia, N. Bissar-Tadmouri, J. Rochelle, E.L. Dadali, M. Zappia, E. Nelis, A. Patitucci, J. Senderek, et al. 2004. Mutations in the mitochondrial GTPase mitofusin 2 cause Charcot-Marie-Tooth neuropathy type 2A. *Nat. Genet.* 36:449–451.